Article Title

Lukas Muessle*

Max Planck Institute for Meteorology
lukas.muessle@mpimet.mpg.de

Abstract

Bla bla bla bla

I. Introduction

I. Literature Review

II. What do we want to do

In this study we want to simulate realistic trajectories of cloud droplets inside a turbulent flow. Cloud droplets staying at the stratocumulus cloud-top will grow more efficiently due to the strong radiative cooling in this region. Therefore, it is important to quantify the residence time of cloud droplets at the cloud-top. For this purpose we will use a Direct Numerical Simulation (DNS), because common Large Eddy Simulation (LES) cannot resolve the smallest turbulent scales, which are an important factor for the realistic representation of trajectories inside a turbulent flow.

III. Lagrangian approach

The common parcel methods describe the evolution of cloud droplets in a implicit way. However, particles inside a turbulent flow can strongly disperse. Two close cloud droplets at a certain point in time can strongly diverge at a second point in time. This effect can not be considered by using a parcel perspective, so that the individual life cycle of a cloud droplet can only be studied in a direct fashion. We want to study the evolution of individual cloud droplets by simulating the movement of each droplet explicitly. Further, the particle method allows us to study the history of the liquid content as in our study the evolution of cloud droplets is only governed by condensation or evaporation and therefore the particles keep memory of the liquid history. Parcels are not capable to keep memory of the liquid history, because the diffusion term smoothed out the liquid content for each parcel.

*A thank you or further information

IV. Limitations

Atmospheric turbulent flows feature a wide range of scales. This large separation can nowadays not be resolved by models, therefore only a subset of length scales can be directly simulated. As already mentioned, we will use a DNS to quantify the contribution of small scale turbulence to the evolution of cloud droplets. By resolving the small scale turbulence we cannot simulate the largest scales of a convective boundary layer (CBL). To attain a broader range of scales, we will use the simplification of infinitely fast thermodynamics. This is a valid assumption for stratocumulus clouds, because this type of clouds tend to mix more inhomogeneous. Computational resources limit the affordable amount of simulated cloud droplets. Still we aim to simulate a large amount of cloud droplets to catch extreme events, like the exceptional growth of some cloud droplets at the cloud top.

II. Methods

I. Formulation

I.1 Eulerian

To study the individual behavior of cloud droplets, a Lagrangian scheme is coupled to an Eulerian scheme. The Eulerian formulation follows Mellado et al. (2010), De Lozar and Mellado (2013a) and De Lozar and Mellado (2013b), who developed a complete set of equations for warm cloud dynamics. This set of equations is based on two conserved variables: total water, q_t and enthalpy, h.
To study the stratocumulus cloud-top it is useful to introduce a cloud-top mixing layer configuration, where the bottom layer consist of cloudy air (moist and cool) covered by a layer of dry and warm air. The mixing is driven by radiative and evaporative cooling close to the boundary between the layers, where a strong inversion is evident. Effects like shear and cloud base fluxes are neglected.

To describe this mixing layer, two reference states q_t^c and q_t^d are introduced, where q_t^c is the total water inside the cloud, denoted by index c and q_t^d the total water content in the top dry free atmosphere, denoted by index d. Assuming infinitely fast thermodynamics it is possible to determine the liquid water as a function of $q_l = q_l(q_t, h)$, since no supersaturation is allowed. According to Albrecht et al. (1985) we define the mixing fraction χ as:

$$\chi = \frac{q_t - q_t^c}{q_t^d - q_t^c}. \tag{1}$$

The enthalpy can be expressed like the total water as:

$$\chi + \delta = \frac{h - h^c}{h^d - h^c}, \tag{2}$$

where δ represents the deviation of the mixing fraction caused by the radiative cooling. As Bretherton (1987) described, it is valid to linearize the buoyancy and liquid water equation, due to that the variations of total water and enthalpy are small. The evolution in the Boussinesq approximation equation can be written for the case that all diffusion coefficients are set equal, which is close to atmospheric values, which simplifies the equations.:

$$\begin{aligned}
&\nabla \mathbf{v} = 0, \\
&\frac{\partial \mathbf{v}}{\partial t} + \mathbf{v} \cdot \nabla \mathbf{v} = -\nabla p + \nu \nabla^2 \mathbf{v} + b\mathbf{k}, \\
&\frac{\partial \chi}{\partial t} + \mathbf{v} \cdot \nabla \chi = \kappa_t \nabla^2 \chi, \\
&\frac{\partial \delta}{\partial t} + \mathbf{v} \cdot \nabla \delta = \kappa_T \nabla^2 \delta - r, \\
&r = \frac{F_0}{\lambda \rho} l \; exp\left[\frac{-1}{\lambda}\int_z^{z_{top}} l(z')dz'\right],
\end{aligned} \tag{3}$$

where $\mathbf{v}$ is the velocity field, p is the modified pressure term divided by a reference cloud density ρ_c, the buoyancy term b is a function of $b = b(q_t, h, q_l)$ with $\mathbf{k}$ as the unity vector in vertical direction, the diffusion coefficient ν represents the kinematic viscosity and κ_T and κ_t the thermal diffusivity and the molecular diffusivity for water. The radiative cooling term r represents the one-dimensional LW forcing, where F_0 is the total cooling per unit area. The normalized liquid water q_l/q_t^c is from now on referred to as $\ell = q_l/q_l^c$. The cloud air density is represented byρ_t and q_l^c is the liquid water content inside the cloud. The extinction length λ is defined by $\lambda = 1/(\kappa \rho_t q_l^c)$, where κ is chosen to match typical atmospheric values. Typical values for λ are $\lambda = 15\,m$ (De Lozar and Mellado, 2013b). The linearized approximation for the liquid water and buoyancy reads:

$$\begin{aligned}
&\xi = 1 - \frac{\chi}{\chi_s} - \frac{\delta}{\delta_s}, \\
&\ell = f(\xi) = \epsilon \ln\left[\frac{\xi}{\epsilon} + 1\right], \\
&\frac{b}{\Delta b} = \chi\left(\frac{1+D}{1-\chi_s}\right) + \frac{\delta}{\delta_b} + (l-1)\left(\frac{D+\chi_s}{1-\chi_s}\right),
\end{aligned} \tag{4}$$

where $\xi = 0$ defines the cloud-dry-air boundary, ℓ the liquid phase, the index s in χ_s defines the saturation value, $\Delta b = b^d - b^c$, $D = -b_s/\Delta b$ represents the normalized buoyancy of the cloud-dry-air mixture at saturation, δ_b is defined by $\delta_b = (c_p^c T^c \Delta b)/g$ and δ_s by $\delta_s = (\delta_b(D + \chi_s))/(a_{sat}(1 - \chi_s))$, where a_{sat} represents a constant, which resolves the interplay of the radiative cooling and the latent heat effects. In the limit $\epsilon \to 0$, $f(\xi)$ tends to the piecewise linear function defined by Bretherton (1987), but with finite second derivative. The piecewise limit is reached if $\epsilon \lesssim 1/16$ is satisfied (Mellado et al., 2009). De Lozar and Mellado (2015) present a more extensive view on this topic.

I.2 Lagrangian

In the Eulerian formulation the evolution of liquid water can be calculated using a diagnostic liquid water equation. The time derivative of the liquid reads:

$$\frac{\partial l}{\partial t} + \nabla(l\mathbf{v}) = \frac{1}{Re}\nabla^2 l + S_{con} - S_{evap}, \tag{5}$$

where the two terms on the left hand side represent the material derivative, the first term on the right hand side reflects the diffusion of liquid, followed by two source terms, the condensation and evaporation which can be calculated like:

$$\begin{aligned}
S_{con} &= \frac{r(l)}{\delta_s}\frac{1}{1 + e^{(-\xi/\epsilon)}}, \\
S_{evap} &= \frac{|\nabla \xi|^2}{Re}\frac{1}{4\epsilon[cosh(\xi/2\epsilon)]^2},
\end{aligned} \tag{6}$$

where $1/(1 + exp(-\xi/\epsilon))$ is equal 1 inside the cloud and zero outside the cloud domain, since condensation only takes place inside the cloud. On the other hand, evaporation is mainly evident at the interface of cloudy air and dry air, and therefore is represented by the function $1/(4\epsilon[cosh(\xi/2\epsilon)^2])$, which has a similar form as a Dirac delta function.

Comparing the thermal fluctuations of cloud droplets ($\kappa_l = 10^{-12}\,m^2 s^{-1}$) to the thermal fluctuations of the gaseous phase ($\kappa_v = 10^{-5}\,m^2 s^{-1}$) (Mellado et al., 2010), it becomes

computational expensive to represent a realistic κ_l, because a high numerical resolution is needed. Due to the difference of several magnitudes, it becomes clear that the molecular diffusion of the liquid phase can be neglect compared to the diffusion of the gaseous phase. However, Direct Numerical Simulations (DNS) and Large Eddy Simulation (LES) keep this term in a modified version. DNS take advantage of an unphysical liquid diffusion to simulate a larger range of scales and the LES uses a modified diffusion term to represent turbulent mixing processes on unresolved scales more accurately.
The modified diffusion term leads to a smoothing out of the liquid field, as the liquid content of a large droplet will be distributed to smaller droplets due to the liquid concentration differences. As this study aims to represent the growth rate for individual droplets, the used diffusion term is physically not correct, because the realistic diffusional interaction between single droplets is close to zero. The diffusion of liquid therefore would mask the growth of lucky droplets. For this reason, we neglect the diffusion term and only use the evaporation and condensation tendencies obtained from the Eulerian diagnostic Equation 5 to represent the evolution of each Lagrangian cloud droplet:

$$\left[\frac{\partial L_i}{\partial t}\right]_{lag} = \left[S_{con} - S_{evap}\right]_{\mathbf{X_i}}, \tag{7}$$

where L_i represents the liquid content and $\mathbf{X_i}$ denotes the position of the Lagrangian particle $(i = 1, 2, ..., N)$ inside the Eulerian domain, so that the tendencies for condensation and evaporation can be interpolated for the particle property.

II. Validation

The position of each particle ($\mathbf{X_i}$) inside the grid domain is used to interpolate the Eulerian tendencies to the Lagrangian particle properties. To interpolate the Eulerian tendencies for velocity, condensation and evaporation we use a trilinear interpolation. This interpolation is validated with several different scenarios and the data showed a good agreement with the Eulerian scheme. Nevertheless, the trilinear interpolation has its limit in the initialize procedure, where strong gradients can be present. Especially the transition region of the cloud boundary is very thin, leading to large gradients over a few grid points. This problem causes an error of about $\approx 6\,\%$ and of course is limited to the boundary between the cloud and the free atmosphere. Numerical errors cause another 4%, so that the maximum error in a reduced number of points is about $\approx 10\,\%$. Overall the convergence is good and allows us to simulate the evolution of cloud droplets using the Eulerian bulk tendencies.

III. Caveats

The comparison of a mixing processes for the Eulerian formulation and the Lagrangian particle formulation revealed too little evaporation for the particle formulation compared to the Eulerian formulation. As an example we show this difference in Figure 1 for the VERDI simulation at timestep of about 8.5 minutes. This effect is introduced by the fact, that the tendencies for all quantities of the Lagrangian scheme are interpolated from the Eulerian scheme.

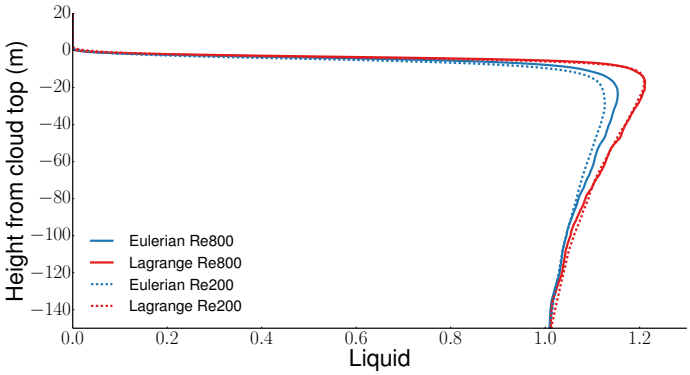

Figure 1: Liquid content over the vertical domain from the cloud top downwards. Solid lines represent a $\mathrm{Re}_0 = 800$ and dashed lines $\mathrm{Re}_0 = 400$. The blue colors indicate the Eulerian formulation, whereas the green colors represent the Lagrangian formulation. The differences between the Eulerian and Lagrangian formulation originates from the diffusion term, which artificially distributes the liquid leading to a higher evaporation rate for the Eulerian formulation. The difference between the two Reynolds numbers for the Eulerian scheme is as well correlated with the diffusion term as the diffusion 6of liquid is higher for the lower Reynolds number.

Before explaining the differences in the evaporative feedback, we should point out that difference Reynolds numbers show different evaporation rates for the Eulerian liquid. This originates from the diffusion term as a lower Reynolds numbers leads to more diffusion, which artificially evaporates liquid at the cloud boundary.
To explain the difference in the evaporative feedback between the Lagrangian and Eulerian scheme, we sketch a characteristic mixing process presented in Figure 2. The left part of the sketch represents the initial condition of a characteristic mixing event. The left box, on the left side of

the sketch, represents cloudy moist air with cloud droplets. Next to the box with cloudy air, dry air from the free atmosphere is entrained into the cloud represented by the right box. This box features no liquid as the air origins from outside the cloud. The entrainment event is followed by a typical mixing process, which is presented on the right side of the sketch. Whereas, the upper boxes (a and b) represent the mixing process for the Eulerian formulation ($\nabla^2 l$) and the lower boxes (c and d) represent the mixing event for the Lagrangian particle formulation ($\cancel{\nabla^2 l}$).
The mixing process leads to a less moist environment in all four boxes, so that the cloud droplets start to evaporate. However, the liquid formulation of the Eulerian scheme features a diffusive term, therefore liquid (cloud droplets) is diffused from box a to b. This leads to evaporation in both boxes (a and b). In contrast to the Eulerian scheme, the Lagrangian scheme does not diffuse any liquid and therefore all cloud droplets stay in the initial box c. This leads to a higher amount of liquid in box c compared to box a (Eulerian scheme), but as we use the Eulerian tendency for the Lagrangian droplets the evaporation tendency is the same as in box a. On the other hand, there is no evaporation in box d, leading to less evaporation compared to box b. This introduces an error for the Lagrangian particle formulation, because the evaporation rate would naturally be higher, due to the higher liquid content in box c.

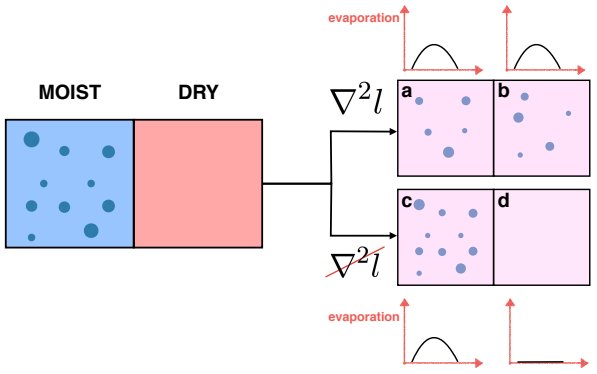

Figure 2: The left side of the sketch represents the initial situation of a cloudy moist environment in the left box and dry entrained air in the right box. The right side of the sketch represents the mixing processes. On the one hand, the Eulerian formulation ($\nabla^2 l$) diffuse liquid from box a into box b, where on the other hand the Lagrangian particle formulation ($\cancel{\nabla^2 l}$) does not diffuse any liquid. Therefore, the interpolation of the tendencies of the evaporation is erroneous, as the liquid content in c is higher as in a.

This uncertainty does not influence the overall study goal, because the largest droplets will not be located in regions with strong entrainment. Nevertheless, this problem should be evaluated in further studies.

IV. Numerics

IV.1 Eulerian setup

All simulations feature a grid of $1024 \times 1024 \times 1024$ grid points. The resolution parameter of $\Delta x/\eta$ is roughly of the order 2.0, with Δx as the grid spacing and η as the Kolmogorov length scale. As stated by Mellado (2010) this resolution is large enough to obtain grid resolution independency for the statistics of interest. The simulated cloud extent and the Kolmogorov length scale are presented in Table 1, where a lower Reynolds number features a larger Kolmogorov length scale but with a larger cloud extent. The simulations feature a continuously growing mixing layer, which prescribes the correlation of the simulation time and the CBL thickness. This leads to a time dependent growth of larger eddies and therefore leading to a wider range of turbulent scales in time. As real stratocumulus clouds do not feature the growth of eddies in such a manner we performed an additional simulation with a second stratification below the cloud top to restrict the continuous growth of the largest eddies. As these simulation are computational expensive, the stratification was only studied using the VERDI reference case with a Reynolds number of $\mathrm{Re}_0 = 200$.

IV.2 Lagragian setup

The computational resources used by the Lagrangian part of the scheme determines the maximum amount of cloud droplets that can be simulated. The overhead due to the Lagrangian calculation can be divided into two parts. The initial overhead scales with the domain size and additional scalars, which need to be communicated for the construction of the halo zones. For a typical simulation of this study 7 additional scalars needed to be communicated, three velocity components and four expressions from Equation 7 and 5. The initial overhead is almost independent of the number of particles and evolves to a initial overhead of roughly 50% in this study. The second portion of the overall overhead is mainly introduced by interpolation calculations and the communication between the processors. Calculations concerning the liquid formulation are optimized to minimize the interpolation error. Some expressions from Equation 7 and 5 like $\nabla^2 l/Re$, ξ, $|\nabla\xi|^2/Re$ and $f(s)/\delta_s$ are calculated in the Eulerian grid and then interpolated into the particle position. In some cases, like calculations of $exp[(-\xi/\epsilon)]$ and $cosh(\xi/2\epsilon)$, the interpolation calcula-

Case	Extent [m]	z^* [m]	η [cm]
Re_0 = 800	270	$\approx$ 255	13.7
Re_0 = 400	450	$\approx$ 345	23.1
Re_0 = 200	750	$\approx$ 570	37.5

Table 1: Horizontal and vertical extent of the simulated cloud as well as the Kolmogorov length scale for each simulation. These scalars quantify the largest and smallest scales resolved in the calculations.

tions were not accurate enough due to the presence of high gradients. This was minimized by first interpolating the ξ field into the particle position and then calculating the functional form for every particle. This procedure enhances the regularity of the calculation but it also increases the communication to 7 particle properties. Taking all these factors into account it becomes obvious that the second overhead scales with the number of particles. The calculation and the communication of the Lagrangian particles roughly need 1/3 of an Eulerian time-step, as the overhead for 10^9 particle is about $\approx$ 30% and for 10^{10} about $\approx$ 300%. Considering two additional scalars for the Lagrangian calculation and the same number of particles as grid points, the overall overhead for the Lagrangian scheme approximately consumes the same amount of time as an Eulerian time-step.

III. Simulation setup

I. Mixing layer

To study the evolution of cloud droplets inside a stratocumulus cloud we use a cloud-top mixing layer configuration, where the upper layer consists of dry and warm air and the layer beneath of moist and cold air. The moist and cold layer represents the cloud layer, whereas the dry and warm air represents the free atmosphere. The mixing layer is driven by radiative and evaporative cooling close to the boundary between the layers, where a strong inversion is evident. The cloud-top mixing layer prescribes the correlation of the simulation time and the CBL thickness. This configuration leads to the time dependent growth of larger eddies and therefore leading to a wider range of turbulent scales in time. A real stratocumulus cloud does not feature the growth of eddies in such a manner, as the largest eddies are already predetermined by the boundary layer depth, so that a quasi steady state is already present. This simulation setup may influence the cloud droplet growth by the time dependent growth of the CBL. Therefore, we implemented a second stratification, which limits the growth of the mixing layer. This second stratification helps to generate quasi steady state circulation inside the cloud domain.

II. Length scale

Todays computational resources do not allow to simulate all atmospheric turbulent flow length scales, therefore only a subset of length scales can be simulated directly. This subset of length scales obviously should include the relevant length scales of the study, which in this case are the scales of radiative cooling and entrainment. Evaporative cooling is related to the entrainment of dry air at the cloud-top and therefore the relevant scales of entrainment are as well the relevant scales for evaporative cooling. De Lozar and Mellado (2013b) pointed out that the important scale of evaporative cooling is between 50 cm and 60 m, whereas radiative cooling is most effective at the cloud-top in a vertical extent of about 15 m. As a result, the simulated scales are centered around the extinction length $\lambda = 15$ m.

III. Reference cases

Two reference cases are simulated for this study. The first reference case is based on the flight measurements of the VERDI campaign. We will use this reference case for the main part of our studies. The second reference case is additionally used to validate our Reynolds independence. The VERDI campaign took place on May 15, 2012 and an arctic stratocumulus cloud at the Beaufort Sea area is measured according to Klingebiel et al. (2014). The cloud layer is defined by a temperature of $T = -5°$C, a total water content of $q_t = 3.15$ g kg^{-1} and liquid water content of $q_{l_c} = 0.25$ g kg^{-1}. The free atmosphere features values of $T = -0.5°$C, $q_t = 2.4$ g kg^{-1} and the measured atmospheric pressure on that day is 905 hPa. The radiation parameter of $F_0 = 60$ W m^{-2} matches the measured data on board the POLAR 5 aircraft and the extinction length scale is as well $\lambda = 15$ m.

The second reference case is based on the flight RF-01 of the DYCOMS-II campaign. The measured cloud of this flight is a subtropical stratocumulus cloud, which featured a temperature of $T = 10.6°$C with a total water content of $q_t = 9$ g kg^{-1} and a liquid water content of $q_{l_c} = 0.45$ g kg^{-1}, the free atmosphere temperature reads $T = 19.1°$C at a atmospheric pressure of 940 hPa, with a

total water content of $q_t = 1.5$ g kg^{-1}. The extinction length scale is set to $\lambda = 15$ m with $F_0 = 70$ W m^{-2} as the energy exchange of the cloud with the atmosphere per unit surface. More detailed information can be found in Stevens et al. (2005).

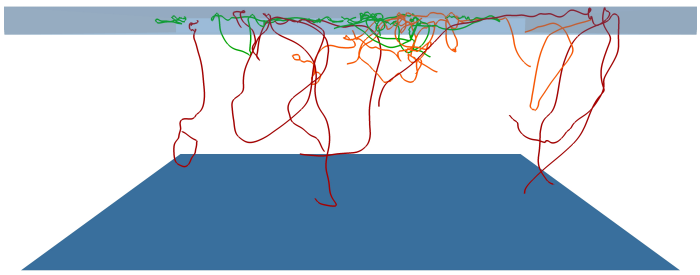

Figure 3: Trajectories for some chosen example cloud droplets. The upper blueish box has a vertical extent of about 2λ, where the radiative cooling is strongest. The lower blue plane represent the second stratification, which limits the growth of the mixing layer. The cloud layer can be imagined between the box and the plane. The example trajectories are classified into three categories. Red trajectories represent cloud droplets, which are mainly driven by the large convective eddies. The orange trajectories represent droplets in a intermediate state, where the stay for a certain amount of time in a vertical level or enter a large convective eddy. Green trajectories represent the lucky droplets, which stay near the cloud top for the hole life cycle.

IV. Results

I. Trajectories

The vertical location of cloud droplets inside a stratocumulus cloud determine the condensational growth rate. As the condensational growth process is the driving force for the growth of small cloud droplets, it is important to understand the movement of the cloud droplets. The majority of droplets will follow the mean flow, which is governed by large turbulent convective movements. Cloud droplets following the mean flow will change their vertical level inside the cloud continuously so that these droplets will not be influenced by strong radiative cooling from the cloud-top. Nevertheless, small scale eddies might help some droplets to escape these large convective movements to reside at a certain vertical level for a longer time period.
In Figure 3 and 4, example trajectories of cloud droplets are visualized. The upper blueish box represents the area at the cloud top where radiative cooling is strongest. This area has a vertical extent of about 2λ, which is about 30 meters. The lower blue plane represent the second stratification, which limits the growth of the mixing layer. The cloud layer can be imagined between the upper box boundary and the lower plane. The example trajectories are classified into three categories and will be explained in the following paragraphs.

The red trajectories represent the movement of the majority amount of cloud droplets. These droplets mainly follow the large convective movements inside the cloud. While the cloud droplets rise inside the cloud, they condensate and grow, whereas when they are in a downward branch they evaporate and shrink. These droplets have no favorite location inside the cloud and spend very little time at the same vertical level. Cloud droplets of the red category experience the strong radiative cooling only for a short period, so that the condensational growth is only slightly enhanced by this process.
The second group of cloud droplets is visualized by the orange trajectories. These cloud droplets represent a intermediate vertical lifecycle. They remain at a certain vertical level for a longer time compared to the red trajectories but still enter once every while a larger eddy to rise and fall inside the cloud. These cloud droplets grow more efficiently compared to the cloud droplets of the red trajectories but still are not influenced by the strong radiative cooling over the whole life cycle.

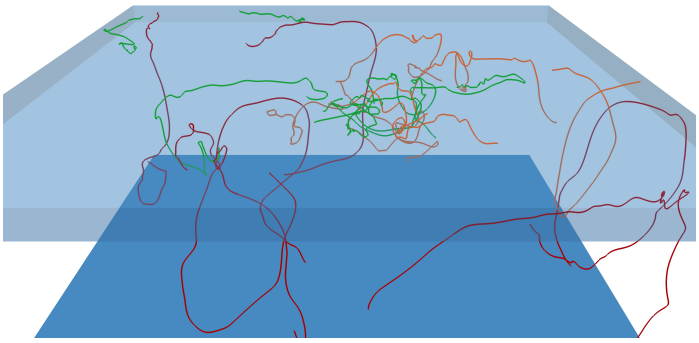

Figure 4: As in Figure 3 but from a different viewing angle.

The last group of cloud droplets is visualized by green trajectories. These trajectories represent cloud droplets, which stay most of the time at the cloud top. Cloud droplets in this area can grow very efficiently, due to the strong radiative cooling at the cloud top. The green trajectories demonstrate that small scale turbulence is important to help a small but considerable number of droplets to stay at the cloud top for an exceptional long time period.

II. Residence time

To understand the behavior of cloud droplets that stay at the cloud-top for an exceptional long time period, we measure the residence times of all droplets at the cloud top. We defined the cloud-top as an area of 2λ in the vertical direction from the cloud boundary downwards and the whole domain in the horizontal direction. The mean amount of cloud droplets staying in the cloud-top region is about 1.37×10^8. In Figure 5 we present the percentile of particles staying in this region for a certain amount of time t divided by the integral time t^* of the system and in Figure **??** we show a similar plot to Figure 5 but with the amount of droplets on the ordinate. Finally, we present the gradient of the amount of droplets in time in Figure 6.

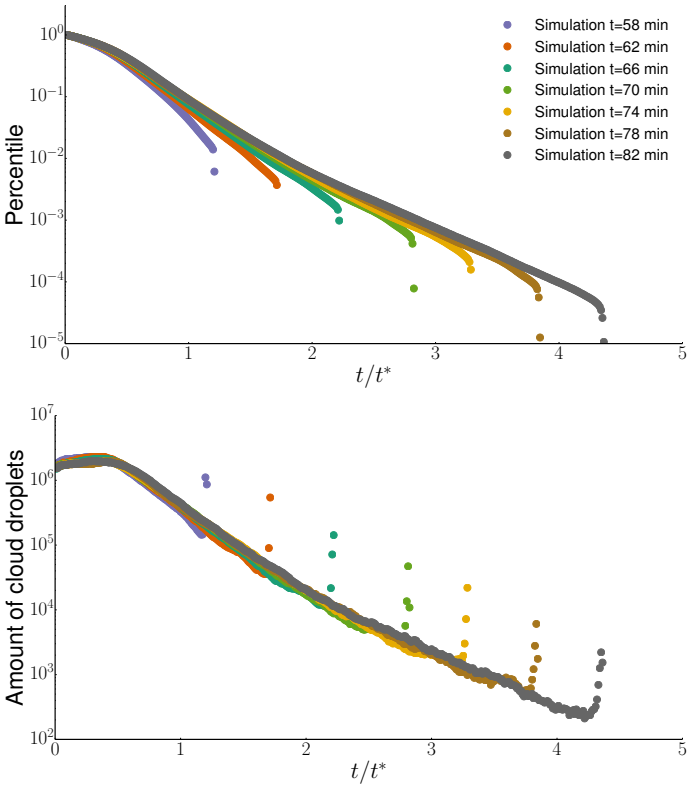

Figure 5: Percentile of cloud droplets staying at the cloud top for a certain amount of t/t^* where t^* ist the integral time scale of the largest convective eddy. The different colors represent the simulation at the given time. The residence times measurements have been started after approximately 49 minutes, which is about 20 minutes after the system touched the second boundary. The plot can be divided into 3 parts, the first part from 0 to $\approx 0.75 - 1$ time-steps shows a rapid decrease of cloud droplets, which stay at the cloud-top. This strong decrease is followed by a weaker decrease from ≈ 1 to ≈ 2.5 time steps and finally the slope stabilizes to a exponential decay for the last part of the curves.

Approximately 80 to 90% of the cloud droplets at the cloud top stay there for $t/t^* \leq 1$ as evident in Figure 5. These cloud droplets are most likely driven by the mean convective eddies as $t/t^* = 1$ represents the typical time period for the largest eddies. We associate these droplets to the red category, because they mainly do not stay at a certain vertical level for a long time period.
The strong decrease in the amount of cloud droplets that stay at the cloud-top is followed by a weaker decrease, which undergoes the exponential decay. The amount of droplets experiencing the weaker decrease ranges from every 100 to every 1000 droplet. The weaker decrease is evident from approximately 1 to 2.5 time-steps. These cloud droplets are represented by the orange trajectories, as the

droplets stay at the cloud top longer as the cloud droplets inside the mean convective movement but are as well dragged out of the cloud top by eddies of the intermediate size.
After this time period the decrease is more stable in time and features an exponential decay. Every 1×10^3 to every 100×10^3 droplet spends about 2.5 to 4.5 time steps at the cloud-top, which is nearly five times larger than time spend at the cloud-top by an average cloud droplet. As Kostinski and Shaw (2005) pointed out, that one lucky droplet every million is needed to initiate rain, we are in a reasonable range for the except growth of some lucky cloud droplets. Besides, there is a strong hint that some lucky droplets stay at the cloud-top for a longer time period. Unfortunately the simulation demands large computational resources. In Figure 5 the cloud droplets of the red catergory are represented by the plateau of droplets.

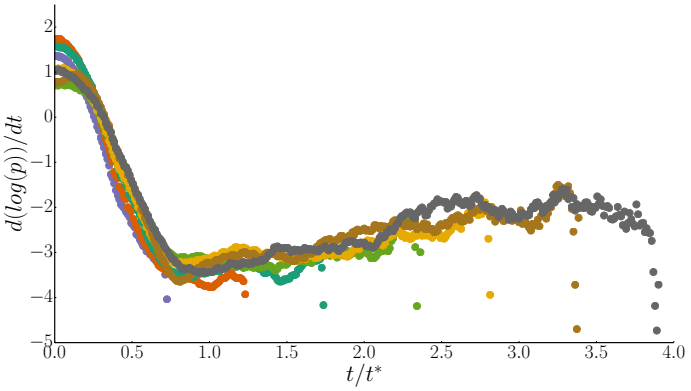

Figure 6: Slope of the curves of Figure 5. A strong increase until around $t/t^* = 0.75$ is evident, followed by a decline until around $t/t^* = 2.5$. After the decline the slope is stabilizes to a value of approximately 2.1 for the rest of the simulation.

To further understand the change in residence times at the cloud top we calculated the derivative of the residence times in Figure 6. It should be noted that the very strong increase at the tail of the slopes originate from cloud droplets, which stayed at the cloud-top from the start of the residence measurements until the considered time-step. The amount of these cloud droplets obviously gets less and less in time as more and more cloud droplets get mixed through out the whole domain.
The first part of the slopes shows a strong increase of the cloud droplets leaving the cloud top, this strong increase has its climax around 0.75 time-steps. As mentioned above, the largest eddies drive the main dynamics of the system and hence leading to this strong reduction of residence times at the cloud-top.
The strong reduction is followed by a decreasing slope. We will call this an intermediate state, where cloud droplets leave the cloud top with a smaller eddy and get recirculated to the cloud-top faster than the ones inside the mean convective movement. These cloud droplets have the chance to catch a second phase at the cloud-top, so that they can stay approximately twice as long as the average one.
This intermediate state is followed by a stable exponential decay of cloud droplets residence times. This means that the residence times of these lucky cloud droplets is fully decoupled from the mean convective motion. These droplets have no memory anymore.

III. Impact of radiative cooling for the cloud droplet size distribution

We will use droplet size distribution (DSD) to represent evolution of the cloud droplets. These DSDs are obtained from the cloud-top with an extent of $1.5 - 3\lambda$. All figures, representing the DSD, show the number of droplets on the ordinate in a logarithmic scale. The logarithmic scale allows for a better investigation of the tail of the distribution, as the extreme growth of cloud droplets is important for this study. The abscissa represents the mass of each cloud droplet divided by the reference mass taken from the reference cases. The different time-steps are represented using the adimensional time $t_0 = (\lambda^2/B_0)^{1/3}$, where for the VERDI campaign the adimensional time reads $t_0 = 49.6$ seconds and for the DYCOMS campaign $t_0 = 47.6$ seconds.

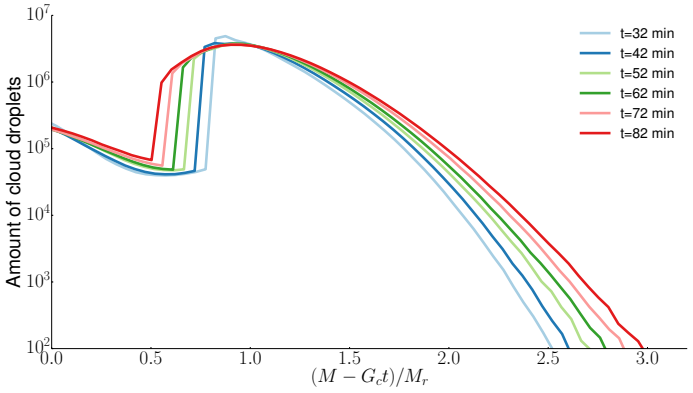

Figure 7: Growth of droplet distribution in time using the adimensional time t0, VERDI $\mathrm{Re}_0 = 200$. The left side of the distributions feature a slight time dependent grow for the smallest droplets, due to the evaporation. The strong jump for intermediate sized droplets originates from two simplification: I) infinitely fast thermodynamics and II) that the cloud base is not physically represented. The peak of the highest number of particles for the mean radius is followed by a exponential decrease which is not time dependent. The tail of the distribution on the other hand is time dependent and features a strong decrease. The tail of the distributions shows a strong condensational growth rate due to radiative cooling. write stratification stuff still

In Figure 7 the evolution of cloud droplets is visualized. For this simulation we used the VERDI reference case and a Reynolds number of $Re_0 = 200$. The continuously growing mixing layer reaches the stratification at a time of about 30 minutes. While the quasi steady state circulation is achieved, the system is cooled artificially, we corrected the DSD by subtracting the additional cooling. The first three blue DSDs represent the continuous mixing layer at a growing stage. The following DSDs represent the stage where the flow already reached the stratification and the quasi steady circulation is achieved.
All droplet size distributions show a pronounced drop right before the mean cloud droplet mass ($M/M_r = 1$), by subtracting the additional cooling the jump moves more to the left for later time-steps. These intermediate sized droplets do not grow efficiently for two reasons. First, infinitely fast thermodynamics do not allow for any supersaturation. Supersaturation would encourage the condensational growth for more cloud droplets, because the mixed super-saturated vapor field could affect a broader region. Hence, the mixing would be more homogeneous. Infinitely fast thermodynamics introduce a strong inhomogeneous mixing. This is justified by the fact that stratocumulus clouds tend to mix more inhomogeneous (Devenish et al., 2012). Second, the cloud-top mixing layer does not represent a physical cloud base. Effects like the activation of aerosols are not simulated. Especially the activation of different sized aerosols at cloud base would lead to a broader spectrum of intermediate cloud droplets sizes. Nevertheless, the study goal is not affected by these simplifications, because the extreme growth of cloud droplets is studied.
The largest number of cloud droplets features approximately a mass similar to the reference mass, which fits with the general distribution of cloud droplets inside the cloud. The peak of the droplet size distribution shows a slightly larger mass than the reference. Since the droplet size distribution is obtained at the cloud-top, where the condensation growth due to the temperature difference inside the cloud is at its maximum, the average cloud droplets are slightly larger than the ones in the center of the cloud.
The following decrease in the droplet size distribution is constant in time until around 1.7 M_r. This intermediate cloud droplets, which are larger than the average but smaller than the largest cloud droplets, stay in the upper region to grow by radiative cooling. The chance to stay at the cloud-top decreases in time due to the convective movement inside the cloud. The number of cloud droplets per M/M_r is exponentially decreasing. The threshold of about 1.7 M_r, where the stronger decrease starts shifts slightly to a larger mass in time. However, this shift is less pronounced in the later time steps and the decrease seems to get more comparative to the exponential decrease.
At the tail of the distribution, the number of droplets per mass decreases rapidly of about an order of 10^4. The slope of this rapid decrease gets weaker as time proceeds, so that more lucky cloud droplets have the chance to survive in the upper cloud region for an exceptional long time period. These lucky droplets grow a lot more by condensation, because they are exposed to radiative cooling for an exceptionally long time.

IV. Influence of scales

The presented results are obtained from a simulation with a Reynolds number of $\mathrm{Re}_0 = 200$ that allowed a longer simulation time. To validate the findings, we will study the Reynolds number dependency in this section. We will use 3 different Reynolds numbers varying from $\mathrm{Re}_0 = 800$ $\mathrm{Re}_0 = 400$ and $\mathrm{Re}_0 = 200$. The comparison of the different Reynolds number simulations is limited to the last time-step of the highest Reynolds number simulation $\mathrm{Re}_0 = 800$, which is approximately around 9 minutes. Regarding the comparison of the simulations the $\mathrm{Re}_0 = 800$ simulation is taken as the reference simulation, due to the better representation of small scale turbulence.
In Figure **??** a strong convergence of both simulations until

about 1.5 M_r is visible. Only at the tail of the distribution of Figure **??** a small deviation is evident. The higher Reynolds number simulation features slightly more cloud droplets with a greater mass. This can be an effect of the smallest eddies in the flow, whose size decreases by increasing the Reynolds number. This suggests that the smallest eddies help cloud droplets to stay at the cloud top.

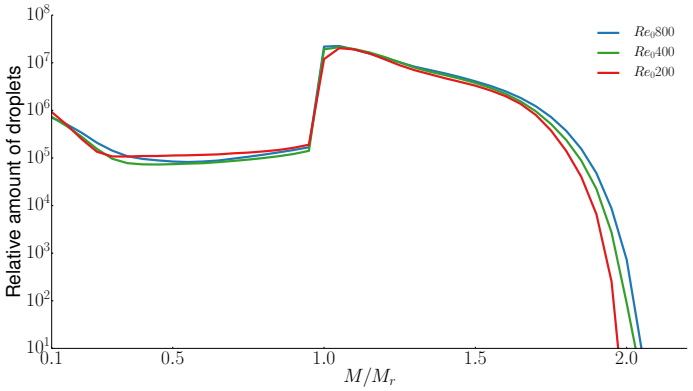

Figure 8: Cloud droplet distribution for the different Reynolds numbers VERDI $Re_0 = 800, 400 \,\&\, 200$. The simulation time is the same as in Figure **??**. The overall convergence is good. However, the tails of the distribution feature small resolution dependence, where the higher resolution tend to have strong growth.

In Figure 8 the convergence of the left part of the droplet size distribution is slightly lower as in Figure **??**, but the divergence is still very small. The lowest Reynolds number $\mathrm{Re}_0 = 200$ simulation captures less evaporation due to entrainment and features consequently less small cloud droplets. This problem is caused by less efficient turbulent mixing of the moist and dry air. Despite of this limitation, the DSDs converge very well except the slight divergence at the tails. As already mentioned before, the slight Reynolds number dependency at the tails is introduced by the size of the limiting smallest eddies. This shows the importance of small scale turbulence for the life cycle of some lucky cloud droplets. The results and conclusions made with a lower Reynolds number simulation are robust, because the extreme growth of cloud droplets is only underestimated, so that we can expect a even stronger growth for a longer simulation with a higher Reynolds number.

V. Discussion

To validate the findings of our simulation we have droplet size distribution measurements from VERDI campaign available. The cloud droplets were measured with a Cloud Droplet Probe (CDP) and a Cloud Imaging Probe (CIP), which covered the size range of about $2 - 960\,\mu$m (Klingebiel et al., 2014). To compare the measured droplet size distribution with the simulation data, measurements from the cloud-top are chosen. As the measurement devices feature a very small sampling area of about $0.27 \pm 0.025\,\mathrm{mm}^2$ (Klingebiel et al., 2014), the droplet size distribution consequently represents less cloud droplets when compared with the simulation results. Therefore, the measurement data is multiplied with a constant value to make the measurement data comparable to the simulation data.

I. Flight measurements

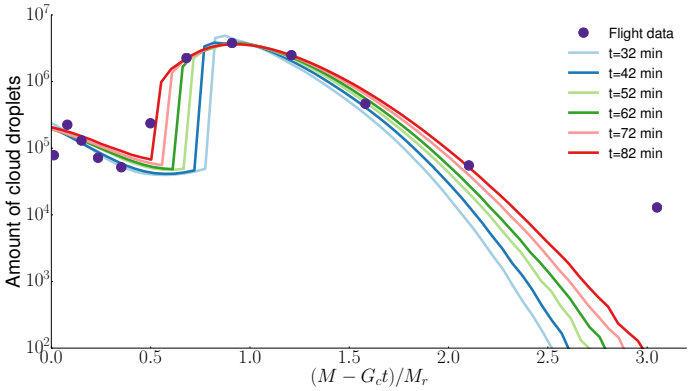

Figure 9: Same droplet size distributions as in Figure 7 and the measured DSD of corresponding flight of the VERDI campaign.

Figure 9 features the same simulation data as Figure 7 with the additional flight measurements. We have a strong convergence of the curves for the constant decrease of droplets in time. In our region of interest three data points are caught very accurately in the region 0.7 to 1.5 M_r and 2 additional points next to these three are still very close. This convergence suggests that the evolution of the cloud droplets simulation is similar as in the measured cloud and that this part of the droplet size distribution is strongly influenced by radiative cooling.

II. Subsection Two

VI. Temporary

Concerning the individual representation of cloud droplets it becomes computational expensive to simulate the realistic thermal fluctuations of cloud droplets, which is negligibly small compared to the thermal fluctuation of the gaseous phase. Nevertheless, DNS and LES commonly keep the diffusion term for liquid in a modified version, to either simulate a broader range of scales or representing turbulent mixing processes on unresolved scales. The modified diffusion term leads to a smoothing out of the liquid field, as the liquid content of a large droplet will be distributed to smaller droplets due to the liquid concentration differences. Therefore, we will neglect the diffusion term for the Lagrangian calculation to better represent the evolution of cloud droplets.

- Movement of particles in cloud is important → radiation → collision → rain [Shaw (2003), Grabowski and Wang (2013), Devenish et al. (2012)]
- LES → low resolution → parcel view Beard and III (1993) → quasi laminar
- Turbulent dispersion (known) → close particles will have different trajectories after short time
- This paper → turbulent dispersion is simulated → 10^9 particles → at cloud top
- Additional → broadening of DSD due to radiative cooling

Turbulent mixing is a key parameter for the formation of clouds and rain (Devenish et al., 2012). The smallest scales may play an important role in defining the macroscopic properties of a cloud (Shaw, 2003). Numerical weather prediction models and climate models can not resolve the smallest turbulent scales and therefore the representation of cloud microphysical processes is still a source of significant uncertainties (Grabowski and Wang, 2013). The role of radiative cooling at the cloud top and the residence time of cloud droplets in this particular area due to small scale turbulence is yet not quantified (Stevens and Feingold, 1996) and might be important. Barkstrom (1978), Austin et al. (1995) and Ackerman (1995) pointed out that radiative cooling can enhance the condensational growth for cloud droplets larger than approximately 10 μm.

Radiative cooling

Longwave radiation is the main driver for stratocumulus cloud dynamics. At the cloud-top a thin region of air is cooled so that the air starts to sink down and drives the dynamics. This thin region is approximately as thick as the extinction length λ, which is a measure for the transparency of a medium. We assume that the cloud behaves like a blackbody and that the longwave radiation is only absorbed and emitted in the vertical direction, which is commonly used in LES codes as the result match observational data (Larson et al. (2007) and Heus et al. (2010)). Furthermore, the total cooling per unit surface F_0 is set constant, because the fluctuation compared to the time scales of the dynamics inside the cloud are negligible small.

Radiative cooling is not only important for the cloud dynamics but also for the growth of the cloud droplets located at the cloud top. These cloud droplets will grow more efficient, due to the higher values in supersaturation. This higher values in supersaturation are a result of the strong radiative cooling which cooles the moist air at the cloud top.

Evaporation

As a result of the downward movement of the cooled air at the cloud top, turbulent eddies at the inversion drag down warm and dry air form the free atmosphere into the cloud layer. These local entrainment events lead to a dilution of the liquid in the cloud layer. The evaporation of cloud droplets affects the liquid water content and the droplet concentration approximately by the same amount. However, the average droplet size is influenced in a minor portion as the mixing events in stratocumulus clouds tend to be more inhomogeneous than in cumulus clouds (Burnet and Brenguier (2007); Devenish et al. (2012)).

From Methods

The evolution equations written in the Boussinesq approximation are

$$\begin{aligned}
&\nabla \mathbf{v} = 0,\\
&\frac{\partial \mathbf{v}}{\partial t} + \mathbf{v}\cdot\nabla\mathbf{v} = -\nabla p + \nu\nabla^2\mathbf{v} + b\mathbf{k},\\
&\frac{\partial q_t}{\partial t} + \mathbf{v}\cdot\nabla q_t = \kappa_t\nabla^2 q_t,\\
&\frac{\partial h}{\partial t} + \mathbf{v}\cdot\nabla h = \kappa_T\nabla^2 h - r,\\
&r = \frac{F_0}{\lambda\rho}\frac{q_l}{q_l^c} exp\left[\frac{-1}{\lambda}\int_z^{z_{top}}\frac{q_l(z')}{q_l^c}dz'\right],
\end{aligned} \tag{8}$$

where $\mathbf{v}$ is the velocity field, p is the modified pressure term divided by a reference cloud density ρ_c, the buoyancy term b is a function of $b = b(q_t, h, q_l)$ with $\mathbf{k}$ as the unity vector in vertical direction, the diffusion coefficient ν represents the kinematic viscosity and κ_T and κ_t the thermal diffusivity and the molecular diffusivity for water. The radiative cooling term r represents the one-dimensional LW forcing, where F_0 is the total cooling per unit area. The normalized liquid water q_l/q_t^c is from now on referred to as $\ell = q_l/q_l^c$. The cloud air density is represented byρ_t and q_l^c is the liquid water content inside the cloud. The extinction

length λ is defined by $\lambda = 1/(\kappa\rho_t q_l^c)$, where κ is chosen to match typical atmospheric values. Typical values for λ are $\lambda = 15\,m$ (De Lozar and Mellado, 2013b).

References

Ackerman, A., 1995: A model for particle microphysics, turbulent mixing, and radiative Transfer in the stratocumulus-topped marine boundary layer and comparisons with measurements. *Journal of the atmospheric ...*, URL http://journals.ametsoc.org/doi/abs/10.1175/1520-0469(1995)052%3C1204%3AAMFPMT%3E2.0.CO%3B2.

Albrecht, B. A., R. S. Penc, and W. H. Schubert, 1985: An Observational Study of Cloud-Topped Mixed Layers. *Journal of the Atmospheric Sciences*, **42 (8)**, 800–822, doi:10.1175/1520-0469(1985)042<0800:AOSOCT>2.0.CO;2, URL http://dx.doi.org/10.1175/1520-0469(1985)042<0800:AOSOCT>2.0.CO2.

Austin, P., S. Siems, and Y. Wang, 1995: Constraints on droplet growth in radiatively cooled stratocumulus clouds. *Journal of Geophysical ...*, **100**, URL http://onlinelibrary.wiley.com/doi/10.1029/95JD01268/full.

Barkstrom, B., 1978: Some effects of 8-12 um radiant energy transfer on the mass and heat budgets of cloud droplets. *Journal of the Atmospheric Sciences*, URL http://journals.ametsoc.org/doi/abs/10.1175/1520-0469(1978)035%3C0665:SEORET%3E2.0.CO%3B2.

Beard, K. and H. O. III, 1993: Warm-Rain Initiation: An Overview of Microphysical Mechanisms. *Journal of Applied Meteorology*, URL http://journals.ametsoc.org/doi/abs/10.1175/1520-0450(1993)032%3C0608:WRIAOO%3E2.0.CO;2.

Bretherton, C., 1987: A Theory for Nonprecipitating Moist Convection between Two Parallel Plates. Part I: Thermodynamics and âĂIJLinearâĂİ Solutions. *Journal of the atmospheric sciences*, URL http://journals.ametsoc.org/doi/abs/10.1175/1520-0469(1987)044%3C1809:ATFNMC%3E2.0.CO;2.

Burnet, F. and J.-L. Brenguier, 2007: Observational Study of the Entrainment-Mixing Process in Warm Convective Clouds. *Journal of the Atmospheric Sciences*, **64 (6)**, 1995–2011, doi:10.1175/JAS3928.1, URL http://dx.doi.org/10.1175/JAS3928.1.

De Lozar, A. and J. P. Mellado, 2013a: Cloud droplets in a bulk formulation and its application to buoyancy reversal instability. *Quarterly Journal of the Royal Meteorological Society*, n/a–n/a, doi:10.1002/qj.2234, URL http://doi.wiley.com/10.1002/qj.2234.

De Lozar, A. and J. P. Mellado, 2013b: Direct Numerical Simulations of a Smoke CloudâĂŞTop Mixing Layer as a Model for Stratocumuli. *Journal of the Atmospheric Sciences*, **70 (8)**, 2356–2375, doi:10.1175/JAS-D-12-0333.1, URL http://journals.ametsoc.org/doi/abs/10.1175/JAS-D-12-0333.1.

De Lozar, A. and J. P. Mellado, 2015: Mixing driven by radiative and evaporative cooling at the stratocumulus top. *In preparation for Journal of the Atmospheric Sciences*.

Devenish, B. J., et al., 2012: Droplet growth in warm turbulent clouds. *Quarterly Journal of the Royal Meteorological Society*, **138 (667)**, 1401–1429, doi:10.1002/qj.1897, URL http://doi.wiley.com/10.1002/qj.1897.

Grabowski, W. W. and L.-P. Wang, 2013: Growth of Cloud Droplets in a Turbulent Environment. *Annual Review of Fluid Mechanics*, **45 (1)**, 293–324, doi:10.1146/annurev-fluid-011212-140750, URL http://www.annualreviews.org/doi/abs/10.1146/annurev-fluid-011212-140750.

Heus, T., et al., 2010: Formulation of the Dutch Atmospheric Large-Eddy Simulation (DALES) and overview of its applications. *Geoscientific Model Development*, **3**, 415–444, doi:10.5194/gmd-3-415-2010.

Klingebiel, M., et al., 2014: Arctic low-level boundary layer clouds: in-situ measurements and simulations of mono- and bimodal supercooled droplet size distributions at the cloud top layer. *Atmospheric Chemistry and Physics Discussions*, **14 (10)**, 14 599–14 635, doi:10.5194/acpd-14-14599-2014, URL http://www.atmos-chem-phys-discuss.net/14/14599/2014/.

Kostinski, A. B. and R. a. Shaw, 2005: Fluctuations and Luck in Droplet Growth by Coalescence. *Bulletin of the American Meteorological Society*, **86 (2)**, 235–244, doi:10.1175/BAMS-86-2-235, URL http://journals.ametsoc.org/doi/abs/10.1175/BAMS-86-2-235.

Larson, V. E., K. E. Kotenberg, and N. B. Wood, 2007: An Analytic Longwave Radiation Formula for Liquid Layer Clouds. *Monthly Weather Review*, **135 (2)**, 689–699, doi:10.1175/MWR3315.1, URL http://journals.ametsoc.org/doi/abs/10.1175/MWR3315.1.

Mellado, J. P., 2010: The evaporatively driven cloud-top mixing layer. *Journal of Fluid Mechanics*, **660**, 5–36, doi:10.1017/S0022112010002831, URL http://www.journals.cambridge.org/abstract_S0022112010002831.

Mellado, J. P., B. Stevens, and N. Peters, 2009: Buoyancy reversal in cloud-top mixing layers. **978 (April)**, 963–978, doi:10.1002/qj.

Mellado, J. P., B. Stevens, H. Schmidt, and N. Peters, 2010: Two-fluid formulation of the cloud-top mixing layer for direct numerical simulation. *Theoretical and Computational Fluid Dynamics*, **24 (6)**, 511–536, doi:10.1007/s00162-010-0182-x, URL http://link.springer.com/10.1007/s00162-010-0182-x.

Shaw, R. a., 2003: Particle -Turbulence Interactions in Atmospheric Clouds. *Annual Review of Fluid Mechanics*, **35 (1)**, 183–227, doi:10.1146/annurev.fluid.35.101101.161125, URL http://www.annualreviews.org/doi/abs/10.1146/annurev.fluid.35.101101.161125.

Stevens, B. and G. Feingold, 1996: Elements of the Microphysical Structure of Numerically Simulated Nonprecipitating Stratocumulus. *Journal of the . . .*, URL http://journals.ametsoc.org/doi/abs/10.1175/1520-0469(1996)053%3C0980%3AEOTMSO%3E2.0.CO%3B2.

Stevens, B., et al., 2005: Evaluation of Large-Eddy Simulations via Observations of Nocturnal Marine Stratocumulus. *Monthly Weather Review*, **133 (6)**, 1443–1462, doi:10.1175/MWR2930.1, URL http://dx.doi.org/10.1175/MWR2930.1http://journals.ametsoc.org/doi/abs/10.1175/MWR2930.1.